Modeling of the monthly distribution of soil erosion and sediment yield in the Tucutunemo Basin, Venezuela

Samuel Cárdenas[a], Adriana Márquez*,[a], Edilberto Guevara[a], Demetrio Rey[b]

[a]*Center of Hydrological and Environment Research, University of Carabobo, Venezuela.*
[b]*Institute of Mathematics and Compute Applied, University of Carabobo, Venezuela.*

Abstract.- This research deals with the modeling of the monthly distribution of soil erosion and sediment yield in the Tucutunemo basin for the year 2015. The remote sensing technics on Landsat satellite images and ASTER global digital elevation model of a spatial resolution of 30 meters are adapted to use USLE (Universal Soil Loss Equation) and Langebein-Schumm models to estimate the erosion. The monthly precipitation is estimated using the statistical spatial prediction models based on the Ordinary Krigging using the records of 23 precipitation gauges. The J-Bessel model is the best adjustment to the precipitation of 30 minutes. It has been found that the soil erosion and yield sediment occur in the high and middle part of the basin. According the location, the precipitation of 30 minutes occurs in a magnitude from high moderately to high during the rainy season. The applied method contributes to detect the specific areas of sediment accumulation into the basin

Keywords: soil erosion; sediment yield; J-Bessel model.

Modelado de la distribución mensual de la erosión del suelo y la producción de sedimentos en la cuenca de Tucutunemo, Venezuela

Resumen.- Esta investigación tiene como objetivo el modelado de la distribución mensual de la erosión del suelo y la producción de sedimentos en la cuenca de Tucutunemo, para el año 2015. Con la finalidad de estimar la erosión, se adaptaron las técnicas de detección remota en imágenes satelitales de Landsat y el modelo de elevación digital global ASTER con una resolución espacial de 30 metros para utilizar los modelos USLE(*Universal Soil Loss Equation*) y Langebein-Schumm. La precipitación mensual se estima utilizando los modelos estadísticos de predicción espacial, basados en Krigging Ordinario usando los registros de 23 indicadores de precipitación. Para la precipitación de 30 minutos, el modelo J-Bessel es el que presenta mejor ajuste. Se ha encontrado que la erosión del suelo y la producción de sedimentos ocurren en la parte alta y media de la cuenca. Así mismo, las precipitaciones de 30 minutos se producen en una magnitud de moderadamente alta a alta, según la ubicación, durante la temporada de lluvias. El método aplicado contribuye a detectar las áreas específicas de acumulación de sedimentos en la cuenca

Palabras claves: Erosión de suelos; Producción de sedimentos; Modelo J-Bessel.

Received: November 25, 2018
Accepted: February 15, 2019

1 Introduction

Until the end of the 1970s, the soil erosion and sediment yield models were used to estimate the lumped occurrence of these hydrological variables. Because of the development of the computer technology, the geographical information system (GIS) capabilities, and the availability of remote sensing products such as the satellite images and digital elevation models (DEM) to the present, the transition from the lumped models to the distributed models has been possible. The lumped models are characterized by two aspects: 1) they assume spatially homogeneous uniform hillslope, and 2) they are empirically based. Among these models have been found USLE [1], RUSLE [2] and EPIC [3]. The distributed models of soil erosion and sediment yield can be classified according to the flow regimen: 1) steady-state and 2) dynamic state. In the first case, the distributed models of soil erosion and sediment yield have the following

*Autor para correspondencia:
*Correo-e:*ammarquez@uc.edu.ve (Adriana Márquez)

characteristics: 1) They are models that adequately represent deposition processes or sedimentation pathways, 2) they are process-based models, 3) they are characterized by the presence of a governing differential equation such as the kinematic wave model. Among these models have been found ANSWER [4], Water Erosion Prediction Project (WEPP) model [5] and the European Soil Erosion Model (EUROSEM) [6]. In the second case, the distributed models of soil erosion and sediment yield have the following characteristics: 1) They are models that adequately represent deposition processes or sedimentation pathways, 2) they are process-based models, 3) they are characterized by the presence of a governing differential equation such as the kinematic wave model and 4) they provide information on peak sediment discharge or the sediment load pattern within a storm. The main model that represents this evolution is the dynamic version of the WEPP known as DWEPP [7].

In recent years, the progress in the GIS tools and the products derived of remote sensing have given as a result the application of the USLE model in the steady-state by estimating the soil erosion from the models evolved from rainfall based erosion prediction, through Soil Conservation Service Curve-Number-based runoff estimations. These USLE applications to estimate the soil erosion precisely on the watershed and basin scale rather at a field scale have been implemented by [8, 9]. The DEM allows to use the terrain elevations to estimate the terrain slope with a spatial resolution that can be adjusted to the field practices, which influences on the topographical factor. The satellite images allow to apply classification techniques to estimate the land use and land cover (LULC) in the study area, which influences on the crop management factor (C), the conservation practice factor (P) and the curve number (CN). This study is carried out on the Tucutunemo river basin, the aims are: 1) to apply the empirical models to estimate the soil erosion and the sediment yield, such as USLE and Langbeing-Schumm model, 2) to determine the areas associated to the source for soil particle detaching and sediment yield.

2 Study area

The study area is the Tucutunemo river basin located in the Aragua State at the central region of Venezuela (Figure 1). The basin area is limited by the following coordinates: 67°19'00"W, 67°29'00"W, 10°02'00"N, 10°08'30". The length of the main stream of the Tuctunemo river is of 27 km. The terrain slope varies as follows: 0-15% (41 km^2, 37%), 15-33% (38 km^2, 35%), 33-54% (25 km^2, 22%), 54->153% (7km^2, 6%). Most part of terrain slope can be classified as of mean to high varying in a range between 5 and 20% [10]. The total area of basin is 110 km^2.

3 Methods

3.1 Estimation of the soil erosion

The soil erosion is estimated using the Universal Soil Loss Equation (USLE) model developed by [1] following the process shown in the Figure 2. The equation (1) estimates A, the average annual soil erosion per unit area (t/ha) from six independent factors: a) R is rainfall erosivity factor (MJ.mm/ ha.h); b) K is the soil erodibility factor (Mg.h/MJ.mm) c) LS is the topographical factor integrated by L, length factor and S, the slope steepness factor; d) C is the crop management factor and e) P is the conservation practice factor.

$$A = R \cdot K \cdot L \cdot S \cdot C \cdot P. \tag{1}$$

a) **Rainfall erosivity factor (R):** the R factor (Figure 3) for n number of periods is calculated using total kinetic energy of a storm (E) for k number of such type of periods using the following equations (2),(3) and (4):

$$E = \sum_{i=1}^{k} E_i, \tag{2}$$

$$EI_{30} = E \cdot I_{30}, \tag{3}$$

$$R = \sum_{l=1}^{n} \left[\sum_{j=1}^{m} (EI_{30})_j \right]. \tag{4}$$

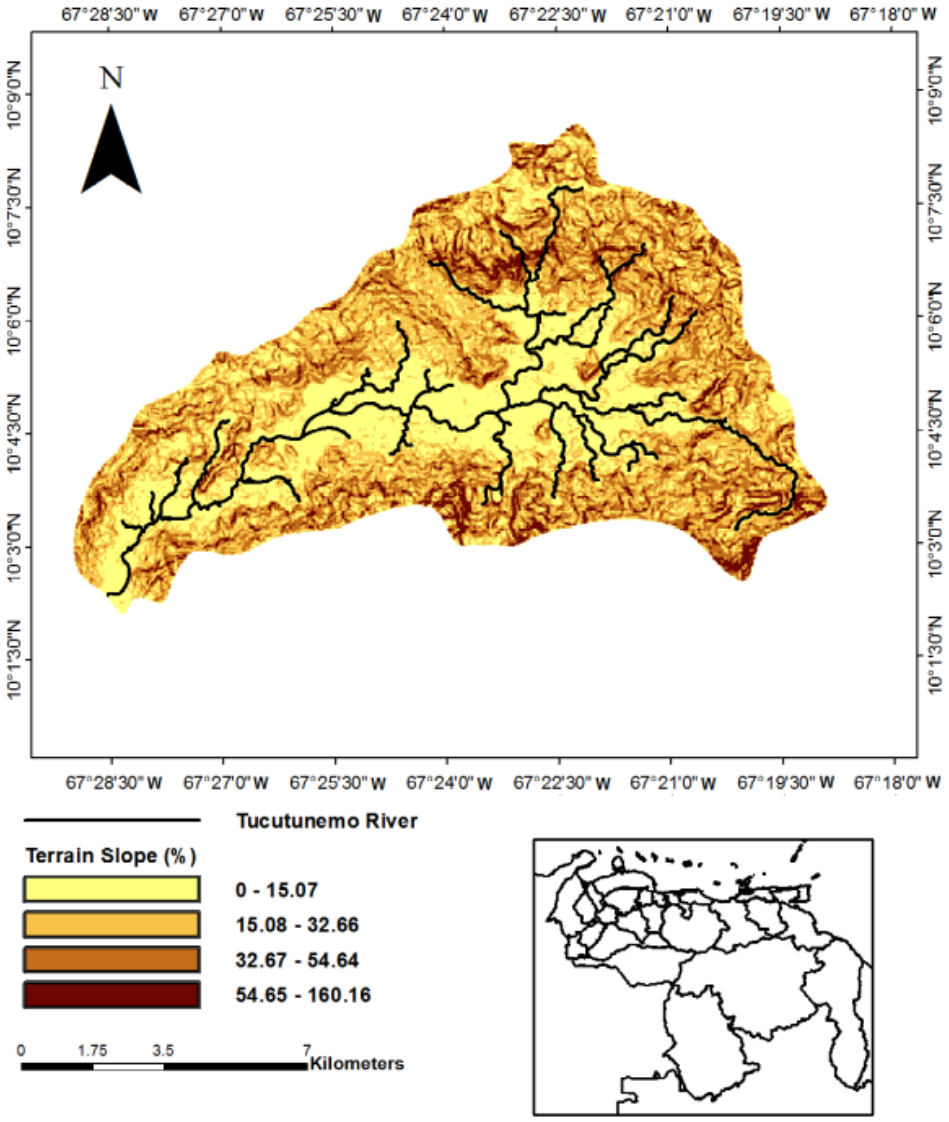

Figure 1: Location of Tucutunemo river basin, Aragua state, Venezuela.

Where, I_{30} is the highest rainfall intensity in any 30 minutes duration (mm/h); EI_{30} is the rainfall erosivity index for storm j; m is the number of storms in n number of periods; R is rainfall erosivity factor (MJ.mm/ha.h) for n number of periods. The kinetic energy for the rainfall periods having constant intensity is estimated using the equation (5) [1]:

$$\begin{cases} E_i = P_i\left(0,119 + 0,0873\log_{10} I_i\right), \\ \textit{if } I_i < 76\vee \\ E_i = P_i\left(0.0.283\right), \textit{ if } I_i > 76\vee \end{cases} \quad (5)$$

Where, E_i is the kinetic energy per area unit (MJ/ha); P_i is the depth of rainfall (mm) and I_i is the intensity of rainfall (mm/h) for a rainfall periods having constant intensity.

The rainfall data is acquired from the records each 5 minutes obtained from station network of 24 rainfall gauges operated in real time by the National Institute of Meteorology and Hydrology (Table 1). The rainfall is accumulated from sequencing periods each 5 minutes to a total of 30 minutes. The selected storm event corresponding to duration of 30 minutes is the maximum total precipitation occurred into each month for 2015.

The models of statistical spatial prediction (SSPM) are applied for predicting the precip-

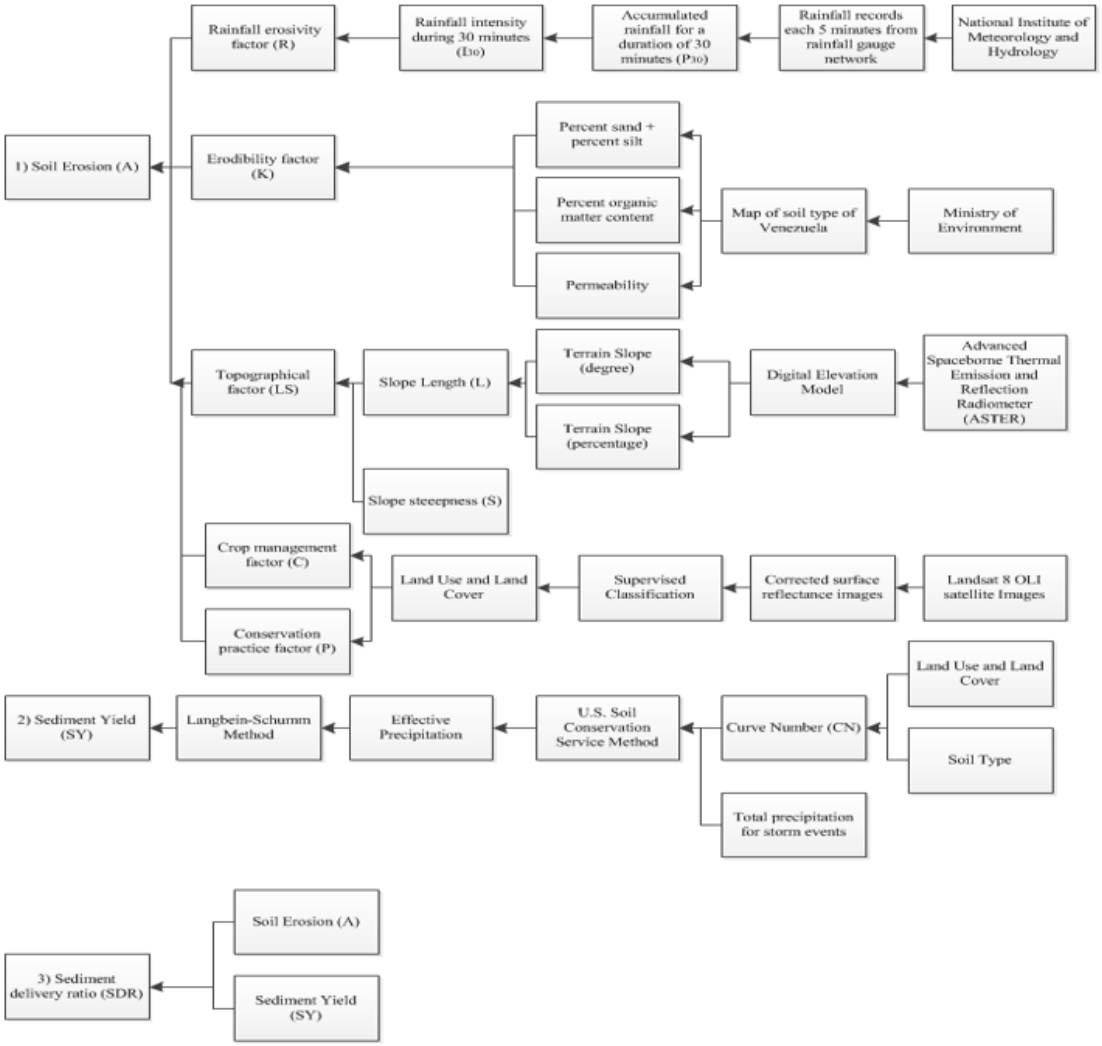

Figure 2: The process of estimating hydrologic variables in the Tucutunemo river basin, Aragua state, Venezuela: 1) Soil erosion (A), 2) Sediment yield (SY), 3) Sediment delivery ratio (SDR).

itation; using the values of the target variable (z) at some new location s_0, being a set of observations of a target variable z denoted as $z(s_1),z(s_2)\ldots,z(s_n)$, where $s_i=(x_i,y_i)$ is a location and x_i and y_i are the coordinates in geographical space and n is the number of observations. The precipitation values represent the target variable. The geographical domain of interest (area, land surface, object) can be denoted as A, represented by the Tucutunemo river basin. It defines inputs, outputs and the computational procedure to derive outputs based on the given inputs: $\widehat{Z}(s_0)= E\{Z/z(s_i),q_k(s_0),\gamma(h),s \epsilon A\}$.

Where $z(s_i)$ is the input point dataset, $q_k(s_0)$ is the list of deterministic predictors and $\gamma(h)$ is the covariance model defining the spatial autocorrelation structure. The type of SSPM used is the statistical model called Ordinary Krigging (OK), whose technique was developed by [11]. The predictions are based on the model refered by the equation (6):

$$Z(s) = \mu + \varepsilon'(s). \quad (6)$$

Where μ is the constant stationary function (global mean) and ε'(s) is the spatially correlated stochastic part of variation. The predictions are made as in [12] introduced to the analysis of point data is the derivation

Figure 3: Monthly rainfall erosivity factor (R) corresponding to the Tucutunemo river basin, Aragua State, Venezuela, during 2015

and plotting of the so-called semivariances — differences between the neighbouring values following the equation (7):

$$\gamma(h) = 1/2E\left[(z(s_i) - z(s_{i+h}))^2\right]. \quad (7)$$

Where z (s_i) is the value of target variable at some sampled location and z(s_{i+h}) is the

Table 1: Rainfall stations in the Tucutunemo river basin.

Identification	Universal Trasversal Mercator (UTM) Zone 19 North	
	X	Y
Maracay	647852	1133364
San juan de los morros	682730	1096657
Guigue	616848	1124032
Barquisimeto	465302	1112800
Acarigua	474393	1055668
Central	720643	1172466
Cumana	370486	1155409
Maturin	479892	1077777
Porlamar	394363	1206934
El vigia	208341	955328
Guanare	419398	996776
Guasdualito	301257	799936
Valera	349492	1018357
Barinas	366124	952685
Valencia-oficina	608178	1131078
Pto cabello base naval	608490	1159760
Campo carabobo	592724	1106863
San diego	616988	1138671
Vigirima	622892	1135723
Hda el manglar	613822	1154779
Agua blanca	626026	1110365
Vivero belen	643956	1105246
Planta de potabilizacion	619290	1112277

value of the neighbor at distance s_{i+h}. The semivariances versus their distances produce a standard experimental variogram. From the experimental variogram, it can be fitted using some of the authorized variogram models, such as linear, spherical, exponential, circular, Gaussian, Bessel, power and similar [13]. The results generated from the application of SSPM for the precipitation data of 30 minutes are shown in Figure 4. The rest of maps are obtained by using the raster calculator tool contained in the menu of spatial analyst tools into the ArcToolbox as a part of menu of available options in the Geographic Information System (GIS) software identified as ArcGIS V10.0.

b) **Soil erodibility factor (K):** the K factor (Figure 5) is the rate of soil erosion per unit of rainfall erosivity index for a specified soil. The K factor was calculated using the following regression equation (8) presented by [14]:

$$K = 2,8 \cdot 10^{-7} \cdot M^{1,14} (12 - a) + \\ + 4,3 \cdot 10^{-3} (b - 2) + 3,3 \cdot 10^{-3} (c - 3). \quad (8)$$

Where, K: soil erodibility factor (Mg.h/MJ.mm); M: particle size parameter (percent silt + percent very fine sand); a: percent organic matter content; b: soil structure code; c: soil profile permeability class. The parameters for the K factor estimating are derived from the Venezuela soil national map created by the Ministry of Environment and available from the website of the Geographic Institute of Venezuela, Simon Bolivar. The extraction of soil type for the Tucutunemo river basin is made using the tool of extraction by mask in ArcGIS 10.0 (Figure 5). Two soil types are found in the Tucutunemo river basin, which are inceptisols (87,75 km^2, 74%) and mollisols (31,2 km^2, 26%) (Figure 5a). Once the soil type is defined, the a and b parameters are mainly obtained from [15]. The average of organic carbon amount in the different depths of profiles in inceptisols order is found varying between 1,1 and 1,44% for a soil depth from 0 to 15 cm [16]. The particle size distribution of inceptisols soil for a depth from 0 to 24 cm determined by Voncir et al.[17], is: sand: 70,45%, silt: 15,06%, clay: 14,49%.The average organic matter amount and average texture for a mollisols soil type are determined by [17, 18], as follows: organic matter: 26 g/kg (2,71%), sand: 120 g/kg (12,5%), silt: 577 g/kg (60,16%), clay: 236 g/kg (24,6%). The percent sand + silt contents and percent organic matter content are shown in Figures 5(b) and Figure 5(c), respectively. For inceptisols and mollisols soils according to the particle size distribution, the permeabilities are 10 m/d and 1 m/d, the medium particle sizes are 0,5 and 0,1 mm, respectively [19]. These parameters a and b to determine the K factor in equation (8) are selected from Table 2 and Table 3. The result of erodibility factor is shown in the Figure 5f.

c) **Topographical factor (LS):** The topography factors such as: slope length (L) and slope

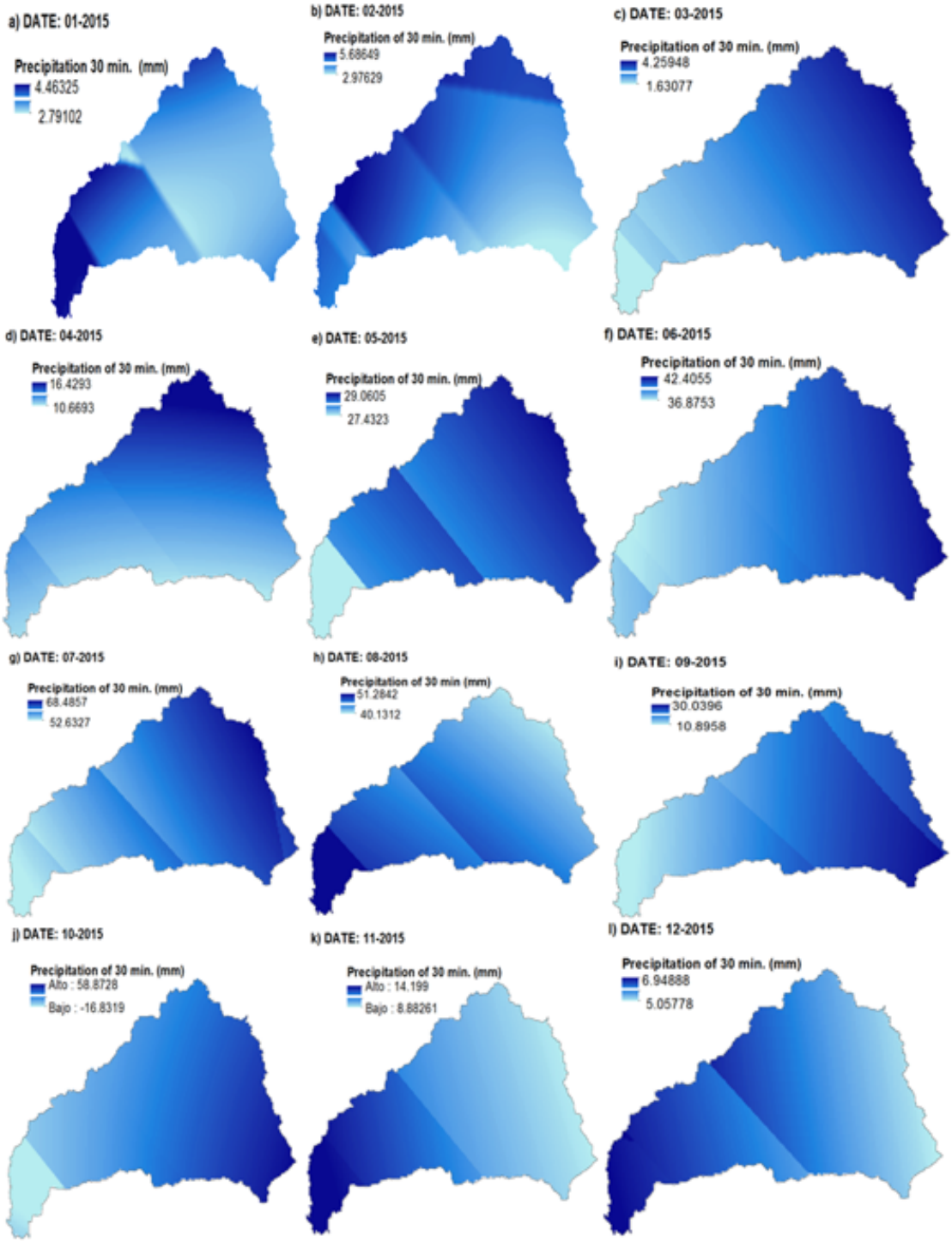

Figure 4: Monthly precipitation measured during 30 minutes corresponding to the Tucutunemo river basin, Aragua State, Venezuela, during 2015

steepness (S) (Figure 6) are calculated using the following equations:

L factor:

It is calculated based on the relationship developed by [1] according the equation (9):

$$L = \left(\frac{\lambda}{22,3}\right)^{m}. \quad (9)$$

Where, λ is field slope length (m); m is the dimensionless exponent that depends on slope,

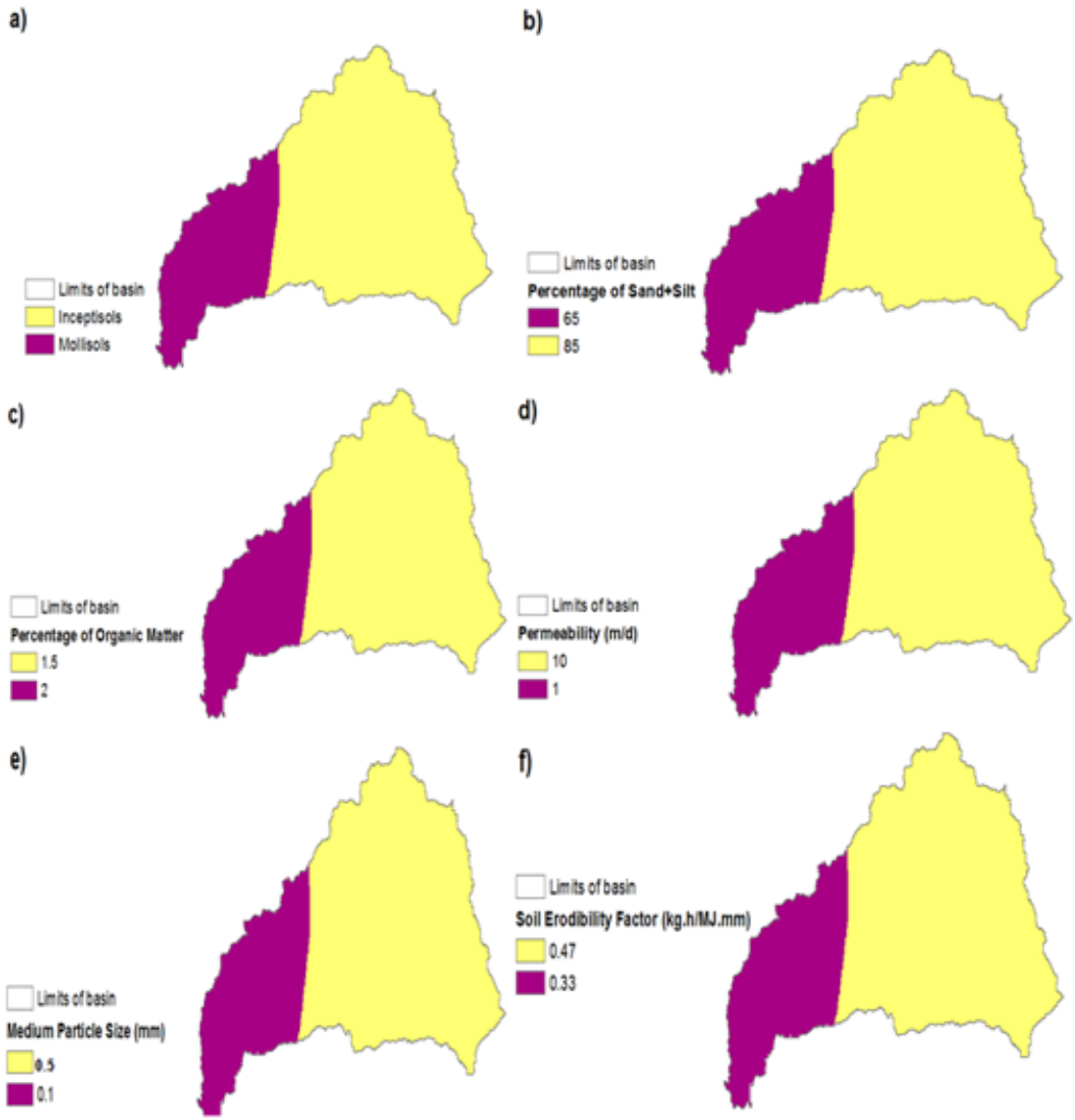

Figure 5: Physical parameters that influence the soil erodibility factor in the Tucutunemo river basin, Aragua state, Venezuela, during 2015.

Table 2: Structure code for different types of soil.

Code	Structure	Particle size (mm)
1	Very fine granular	<1
2	Fine granular	1-2
3	Medium or coarse granular	2-10
4	Blocky, platy or massive	>10

Table 3: Structure code for different types of soil.

Code	Description	Permeability rate (mm/h)
1	Rapid	>130
2	Moderate to rapid	60-130
3	Moderate	20-60
4	Slow to Moderate	5-20
5	Slow	1-5
6	Very slow	<1

being 0,5 if slope > 5%, 0,4 if slope < 5% and > 3%, 0,3 if slope ≤ 3% and > 1%, 0,2 if slope ≤ 1%. The field slope length (λ) is adjusted in the map of digital elevation model to grid size of 100 m based on the recommendation made

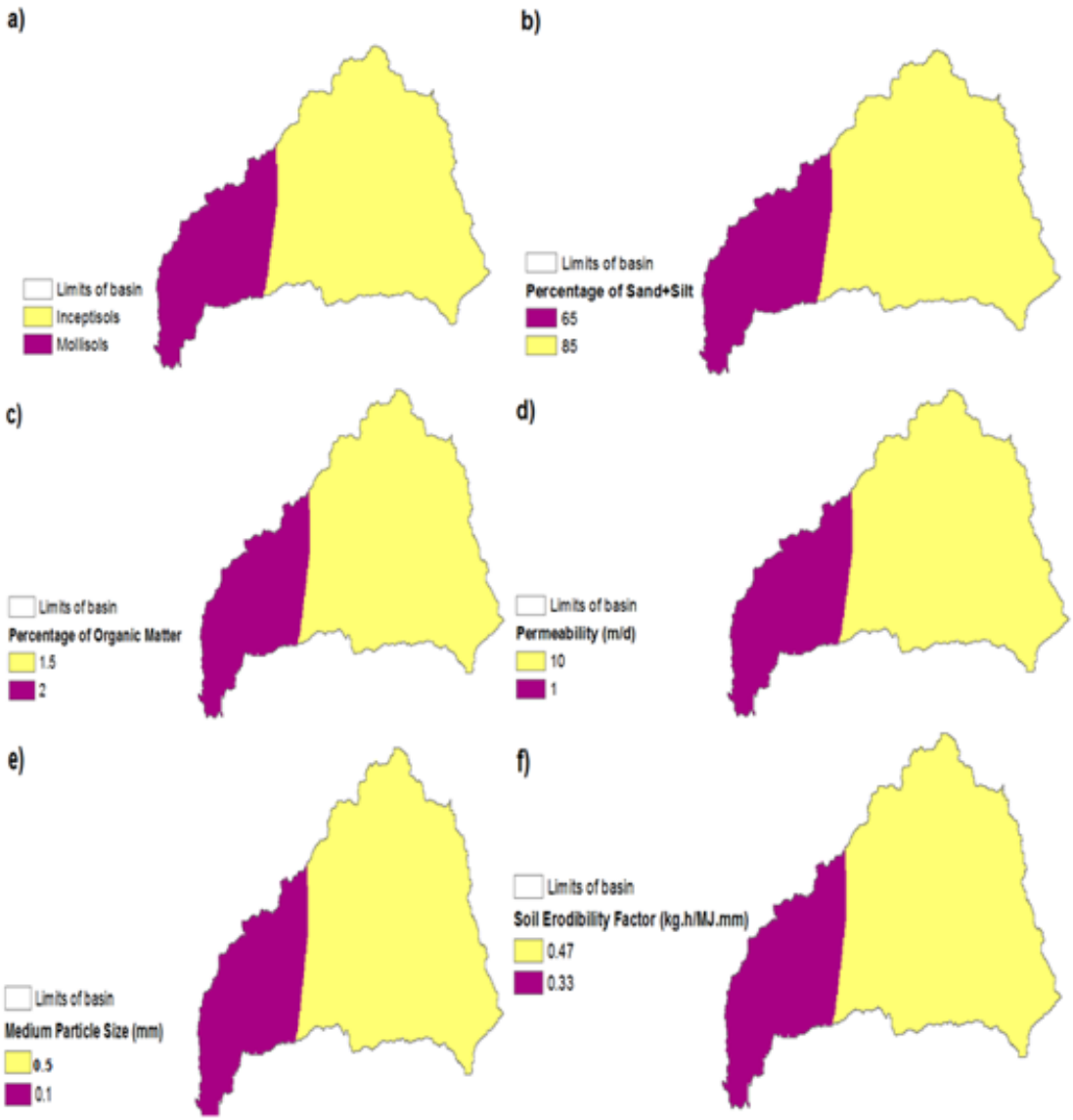

Figure 6: Physical parameters that influence the topographical factor in the Tucutunemo river basin, Aragua state, Venezuela, during 2015: a) Terrain elevation (masl), b) Terrain slope (degree), c) Terrain slope (%), d) topographical factor (LS).

by previous researchers [9]. This adjustment of grid size is achieved by applying a raster resampling technique contained in ArcGIS 10.0, and applied on a digital elevation model (DEM). The gridded data is derived by ASTER (Advance Spaceborne Thermal Emission and Reflection Radiometer) Global DEM as one of the product generated by the METI and NASA agencies (Figure 6a). This DEM is downloaded from the web site: `https://earthexplorer.usgs.gov/`. The entity identification is ASTGDEMV2_0N10W068, the acquisition date is 2011/10/17, the resolution is 1 arc-second, the sensor type is GDEM, the ellipsoid is WGS84 and the unit is degree. The map of parameter m is generated by applying the condition on the slope map in the raster calculator tool of ArcGIS 10.0. The percent slope map is obtained from the surface tool in GIS software (Figure 6c), which requires to introduce a digital elevation model (DEM).

S factor:

It is estimated using the equation (10) having length of the slope higher than 4 m [20].

$$\begin{cases} S = 10,8 \cdot sin(\theta) + 0,03, for\ slope < 9\%, \\ S = 16,8 \cdot sin(\theta) - 0,05, for\ slope > 9\%. \end{cases} \quad (10)$$

Where, θ represents angle of the slope (degrees). The degree slope map is obtained from the surface tool in GIS software using ASTER GDEM (Figure 6b). The (LS) topographical factor map is obtained by the product of slope length (L) and slope steepness (S), and is shown in the Figure (6d).

d) **Crop management factor (C):** the C factor (Figure 7) depends on the land use and land cover (LULC) shown in Figure 8. The map of land use and land cover is obtained by using the maximum likelihood algorithm into the supervised classification tool into ENVI v.4.7 software applied on the of surface reflectance image of Landsat 8 OLI satellite. The satellite images are acquired from the Landsat Collection Level-2, which is based on the surface reflectance (Figure 9). The images have been downloaded from the web site: `https://earthexplorer.usgs.gov/`. The selected satellite was Landsat 8 Operational Land Imager (L8 OLI). The scene is identified under the world reference system according to the following raw and path: 004, 053, respectively. The criterion for selecting of the Landsat images is the lowest coverage of clouds, aerosols and haze. The clouds and their associated shadows, aerosols and haze obstruct the ground view; causing atypical values in the reflectance observations through time. This can lead to confusion of the land use and land cover (LULC) change detection and the analysis of the reflectance trends (Figure 8).
The dependence of the cloud free images restricts the sampling opportunities to the dry season in the tropics [21]. Images affected by clouds, aerosols and haze often contain a large number of free pixels that can be used. The image represents the LULC condition during the dry and rainy season. In Venezuela, the dry period begins in November or December and ends in April or May while the rainy season begins in April or May and ends in November or December [22]. The image characteristics acquired according to the satellite are identified as follows (Table 4): a) the scene identification code: LC80040532015008LGN01, b) the acquisition date: 2015-01-08, c) the cloud coverage:23,98, d) the image quality: 9, e) the angle of sun azimuth: 140,83164216 and f) the angle of sun elevation: 48,15079950. The parameters of map projection according to the United State Geological Survey (USGS) are: a) Projection: Universal Transverse Mercator (UTM), b) Datum: World Geodetic System 1984 (WGS84), c) UTM Zone: 19 N and e) Resample Method: Cubic Convolution.

e) **Conservation practice factor (P):** the P factor (Figure 10) depends on the land use and land cover (LULC) shown in Figure 8.

3.2 Estimation of sediment yield

The sediment yield (SY) is estimated using the Langbeing-Schumm model following the method shown in the Figure 2. This method is also used in watersheds that only have information on effective precipitation. The production of sediments per unit area is estimated according the equation (11) [10]:

$$SY = \frac{10P_e^{2,33}}{1 + 0,0007P_e^{3,33}}. \quad (11)$$

Where, q_s (ton/mile^2), P_e is the effective annual precipitation in inches, can be calculated according to the method of the United States Soil Conservation Service (US-SCS). The US-SCS method requires information on the classification of soils, land use, treatment or practice and the hydrological condition to determine the Curve Number (CN). From the curve number, the storage of water in the soil (S) and the effective precipitation are estimated. The curve number for the wet soil condition (CN III) is shown in Figure 12. The effective precipitation and the sediment yield in the Tucutunemo river are shown in Figure 13 and Figure 14.

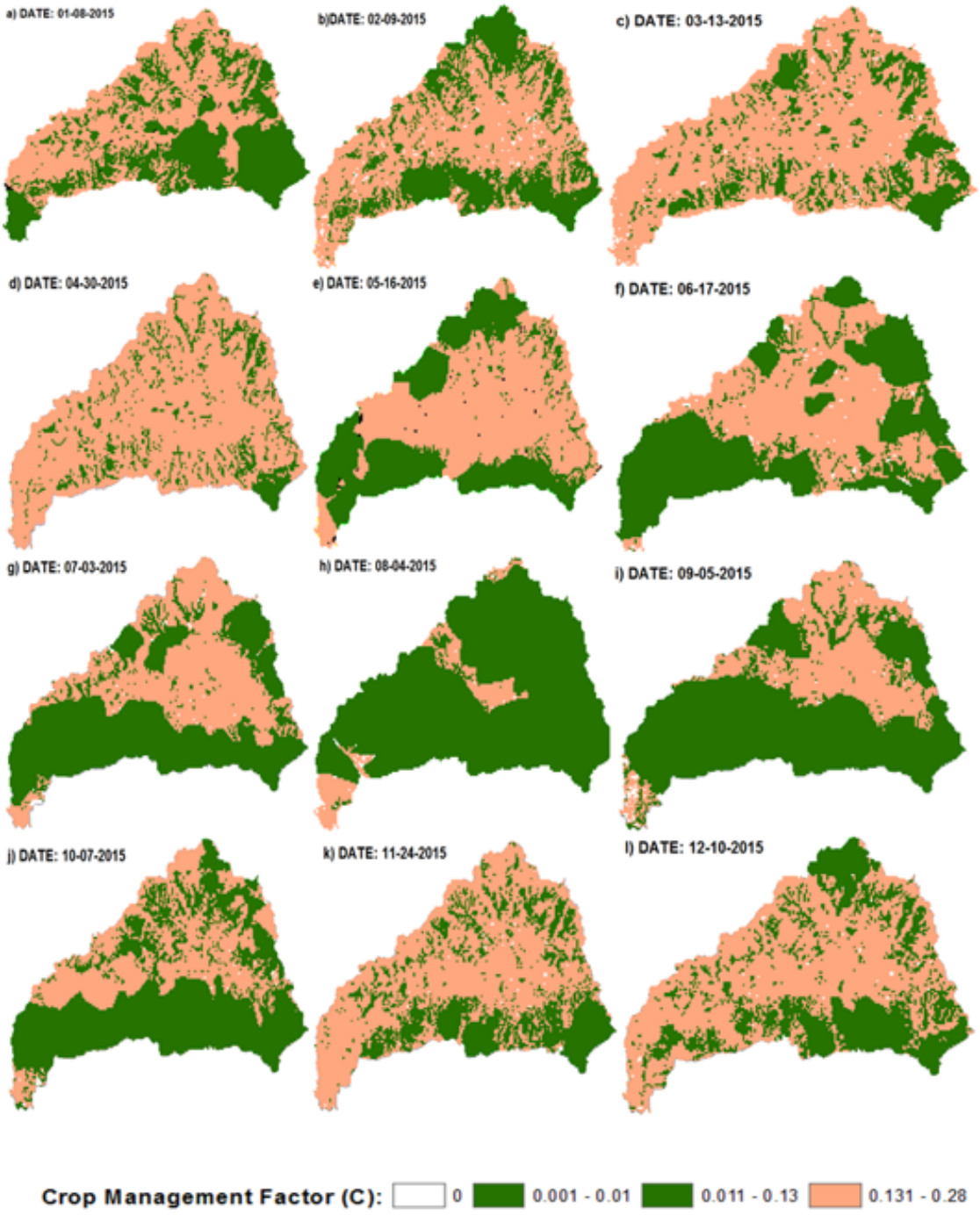

Figure 7: Crop management factor (C) in the Tucutunemo river basin, Aragua state, Venezuela, during 2015.

3.3 Sediment delivery ratio (SDR)

The SDR is a fraction of the eroded soil from the source area transporting to the sink area with surface flow. The equation (12) is a mathematical formulation for estimating SDR, where SY represents the observed sediment yield at the outlet of the watershed and A represents the estimated average annual soil erosion using USLE for the same watershed [23]:

$$SDR = \frac{SY}{A}. \tag{12}$$

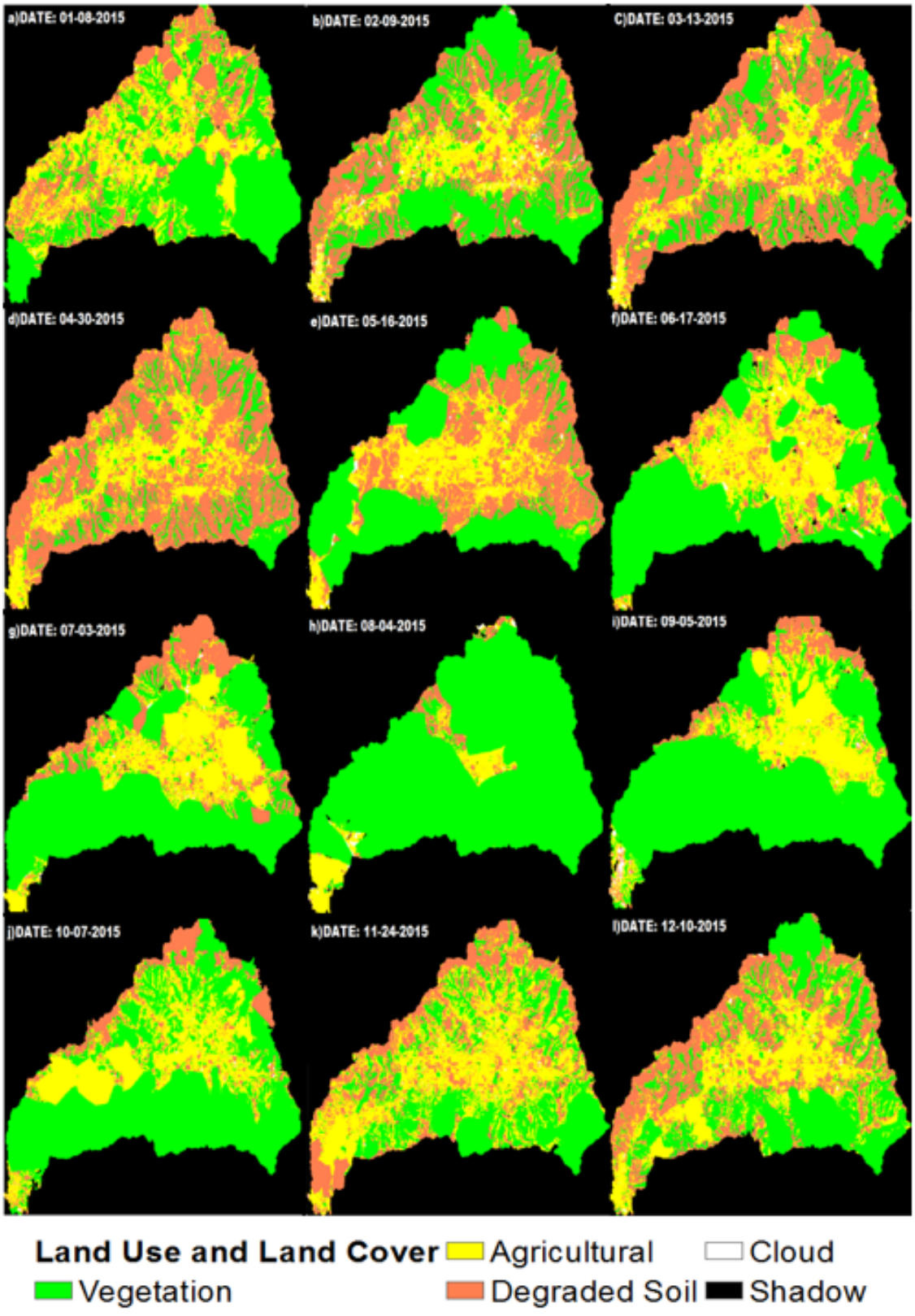

Figure 8: Monthly Land use and land cover corresponding to the Tucutunemo river basin, Aragua State, Venezuela, during 2015

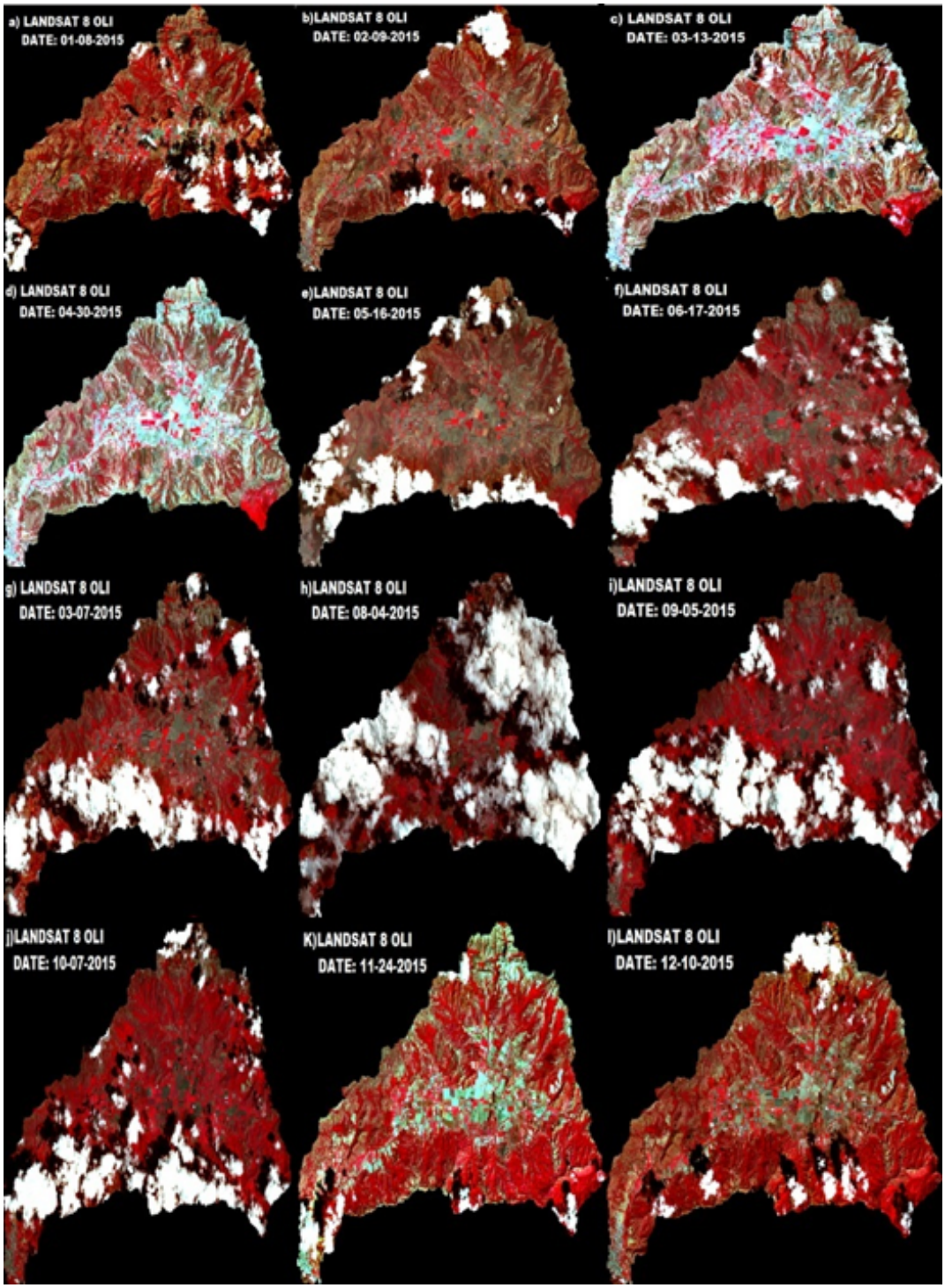

Figure 9: Landsat satellite monthly images corresponding to the Tucutunemo river basin, Aragua State, Venezuela, during 2015.

3.4 Geostatistical modeling of annual soil erosion and annual sediment yield

The type of statistical spatial prediction model used is the statistical model called Ordinary Krigging (OK), whose technique was developed by [11].

Table 4: Images of Landsat 8 OLI satellite.

(1)	(2)	(3)	(4)	(5)	(6)
LC80040532015008LGN01	2015-01-08	23,98	7	140,83164216	48,15079950
LC80040532015040LGN01	2015-02-09	15,00	8,66	130,27865461	52,04329093
LC80040532015072LGN01	2015-03-13	34,78	9	113,66554010	59,30694516
LC80040532015120LGN01	2015-04-30	7,53	9	76,58961361	65,18667019
LC80040532015136LGN01	2015-05-16	45,04	7	66,57532548	64,42909368
LC80040532015168LGN01	2015-06-17	53,52	7	58,47092498	62,01125773
LC80040532015184LGN01	2015-07-03	25,12	9	59,91182760	61,50572841
LC80040532015216LGN01	2015-08-04	35,90	9	71,91635868	62,81459372
LC80040532015248LGN01	2015-09-05	24,10	9	95,64722616	64,90714235
LC80040532015280LGN01	2015-10-07	14,65	9	124,07891462	62,74979513
LC80040532015328LGN01	2015-11-24	7,88	9	144,78160997	52,42420107
LC80040532015344LGN01	2015-12-10	12,71	9	145,27981631	49,69824493

(1) the scene identification code, (2) the acquisition date, (3) the cloud coverage, (4) the image quality, (5) the angle of solar azimuth and (6) the angle of solar zenith.

4 Results

4.1 Results of estimation of the soil erosion

The results of monthly soil erosion maps and its factors during 2015 are shown in Figures 3 to 11.

a) Results of rainfall erosivity factor (R) (Figure 3), the main variable to estimate the rainfall erosivity factor is the precipitation of 30 minutes. The results for the precipitation of 30 minutes from January to December 2015 are shown in Figure 4. The precipitation of 30 minutes in the dry months is similar varying between 1,63 mm and 14,19 mm (Figures 4a, 4b, 4c, 4k and 4l). The precipitation of 30 minutes varies between 10,67 and 68 mm in the rainy months (Figures 4d-4h). The statistical spatial prediction model (SSPM) of monthly precipitation is the J-Bessel function. This function is fitted to the observed precipitation with a gradient that varies between 0,4 and 0,75 (Table 5). The equation is identified by the following coefficients in a general structure: a·Nugget+b·(J-Bessel(c, d)). The values of coefficients vary as follows (Table 5): a: between 0 and 119,36, b: between 14,152 and 492,47, c: between 31797 and 558150, d: between 0,01 and 1,9944. The coefficient a is associated with the no spatial correlation. The coefficient b is associated with C_0+ C_1 term, which is the sill variation. The coefficient c represents the maximum distance between stations of neighbor precipitation observations. The coefficient d represents the parameter of the J-Bessel function. There is pattern in the SPPMs for the dry season, associated with the first months of the each year. In all cases, the semivariances are smaller at shorter distance and then they stabilize at some distance. The results for the rainfall erosivity factor (R) from January to December 2015 are shown in Figure 3. The rainfall erosivity factor in the dry months varies between 0,93 and 19,79 MJ.mm/ha.h (Figures 3a, 3b, 3c, 3k and 3l). The R factor varies between 15,46 and 447,43 MJ·mm/ha·h in the rainy months (Figures 3d-3h). During the dry season, the precipitation of 30 minutes and R factor are higher in the middle and low regions of Tucutunemo basin.

During the rainy season, the precipitation of 30 minutes and R factor are higher in the high and middle regions of Tucutunemo basin.

b) Results of erodibility factor (K) the erodibility factor is estimated by physical parameters which are indicated in the Figure 5. The soil type consists of two classes (Figure 5a): inceptisols and mollisols. Inceptisols comprise the most part of area of Tucutunemo river basin reaching a 74% of total area, from the high to the middle part of basin. Inceptisols and Mollisols are a soil order in USDA soil taxonomy. According to the [15], the central concept of Inceptisols is that of soils of humid and subhumid regions that have altered horizons that have lost bases or iron and aluminum but retain some weatherable

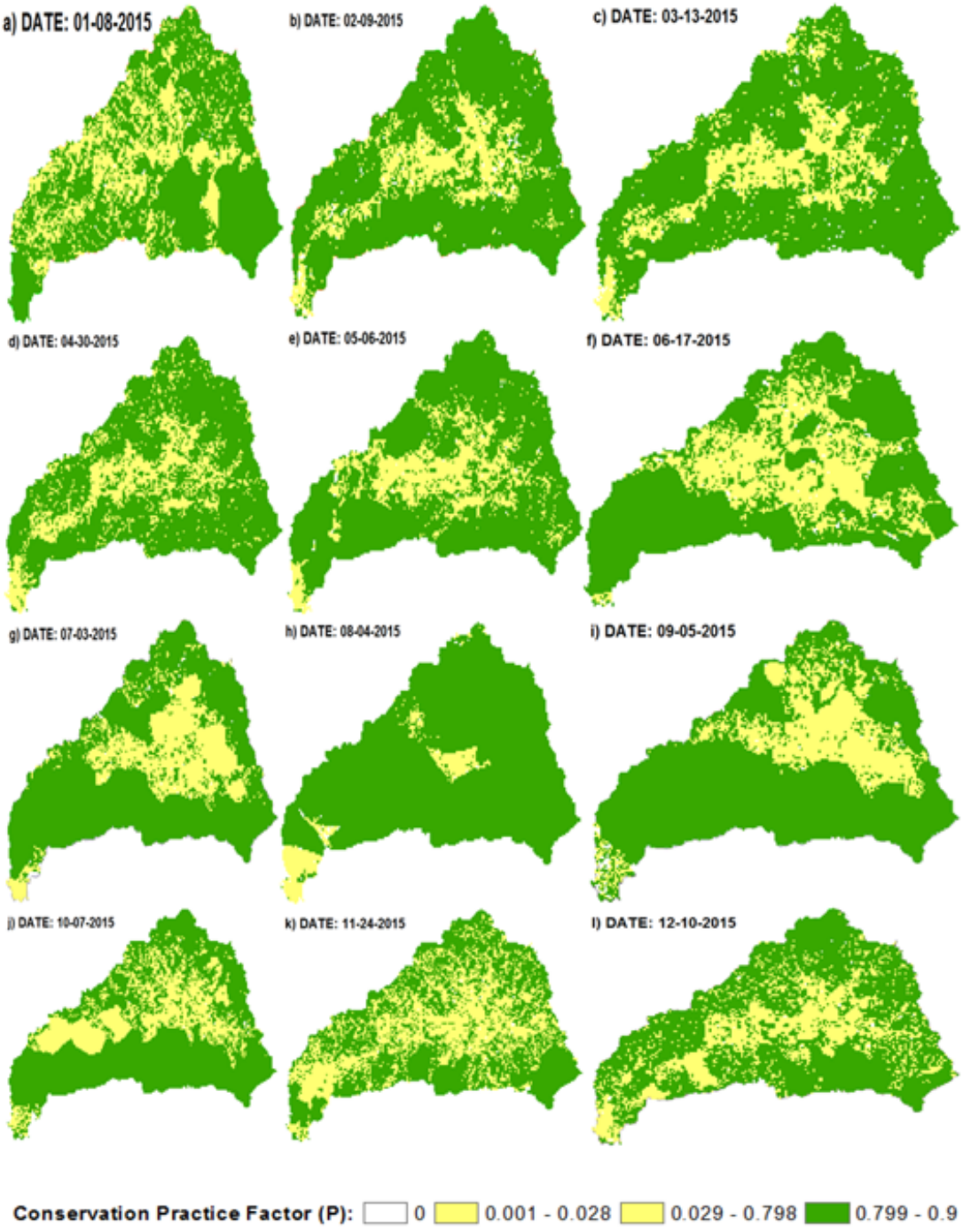

Figure 10: Conservation practice factor (P) in the Tucutunemo river basin, Aragua state, Venezuela, during 2015.

minerals. They do not have an illuvial horizon enriched with either silicate clay or with an amorphous mixture of aluminum and organic carbon. Mollisols comprise 36% of total area of Tucutunemo river basin, in the low part of basin, near to the Valencia Lake. This is the zone where it is developed the agricultural activity. According to the [15], the central concept of Mollisols is that of soils that have a dark colored surface horizon and are base rich. Nearly all

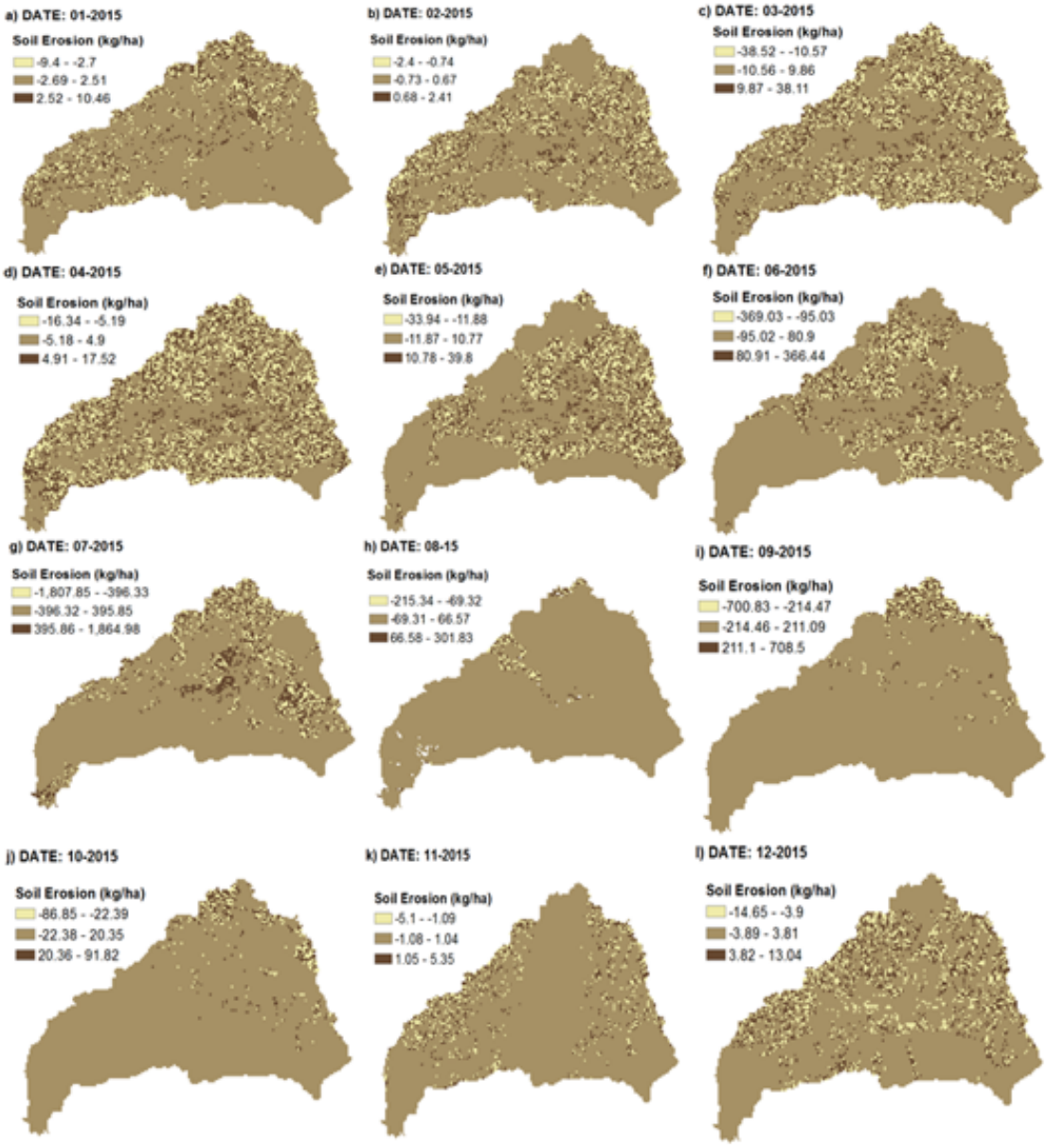

Figure 11: Soil erosion (A) in the Tucutunemo river basin, Aragua state, Venezuela, during 2015.

have a mollic epipedon. Many also have an argillic or natric horizon or a calcic horizon. A few have an albic horizon. Some also have a duripan or a petrocalic horizon. The Inceptisols and Mollisols contain 85% and 65% of silt and sand, 1,5 and 2% of organic matter, 10 and 1 m/d of permeability, 0,5 and 0,1 of medium particle size, respectively. These physical parameters allow to estimate the erodibility factor for a Inceptisol and Mollisol soil as 0,47 and 0,33 kg·h/MJ·mm.

c) Results of topographical factor (LS): The topographical factor is represented by the terrain elevation and the terrain slope. The spatial distribution of the terrain elevations, slopes, and topographical factor varies between (Figure 6a, 6b, 6c): 1) 503 and 704 masl, 0 and 12%, -35 and 28,3 (38,65 km^2, 32,5%), 2) 704 and 902 masl, 12 and 25%, -18,3 and 2,73 (38,65 km^2, 32,5%), 3) 902 and 1124 masl, 26 and 42 %, 2,74 and 21,85 (32,93 km^2, 27,7%), 4) 1124 and 1687 masl, 42 and 94 %, 21,86 and 45,42 (8,44 km^2, 7,09%). The agricultural activity is developed under the first condition.

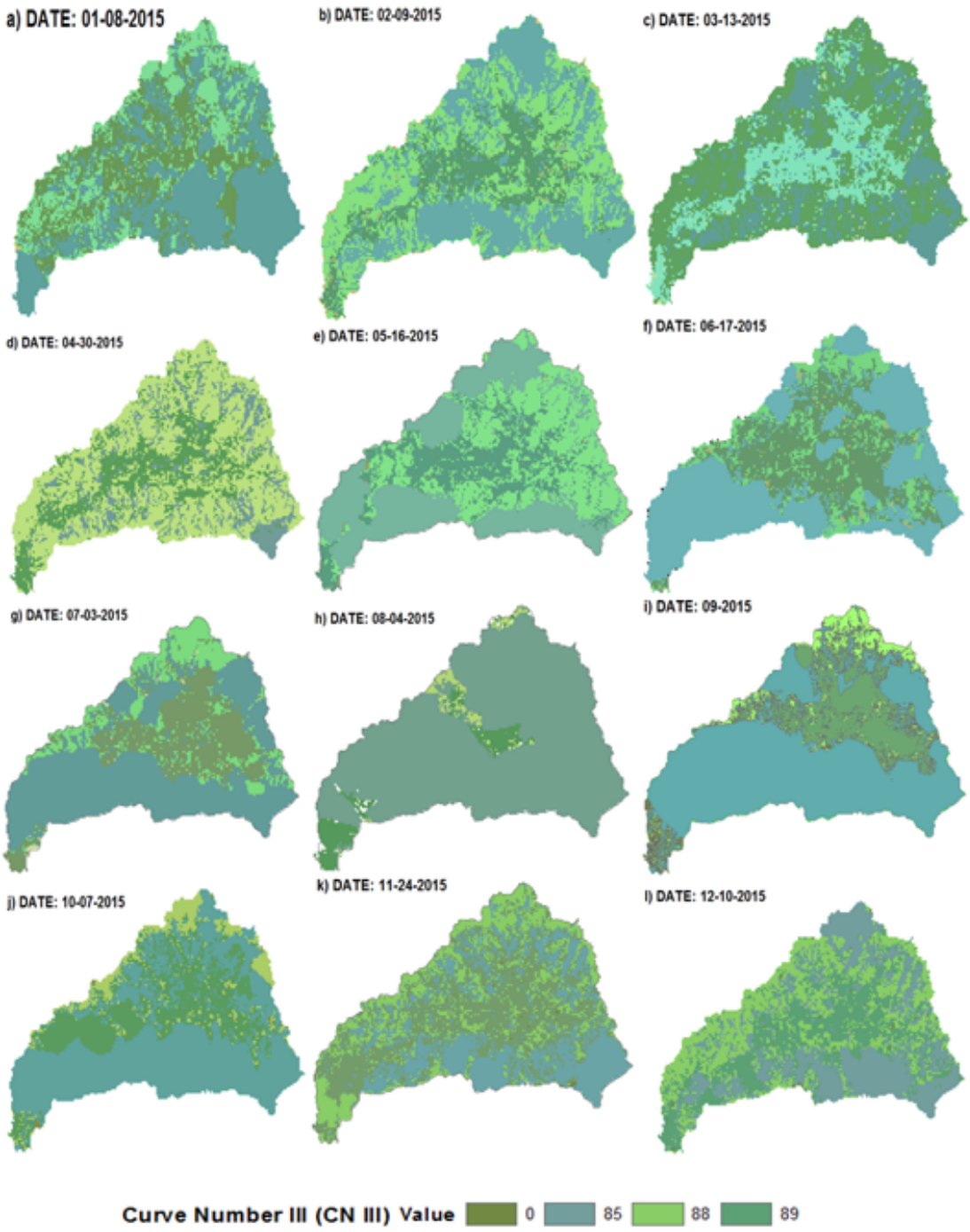

Figure 12: Curve Number (CN III) in the Tucutunemo river basin, Aragua state, Venezuela, during 2015.

d) Results of crop management factor (C) the results of C factor require los results obtained on the land cover and land use derived from Landsat 8 OLI satellite images. These images are shown in Figure 7, where the Tucutunemo river basin is represented from January to December for 2015. The images are shown in false color using the combination of the spectral bands: 5, 4 and 3. The red color is representing the vegetation coverage, which is the most part of the area. Toward the central region of the basin in brightness tone is observed the agricultural uses, which represents the main activity in the Tucutunemo river basin. The

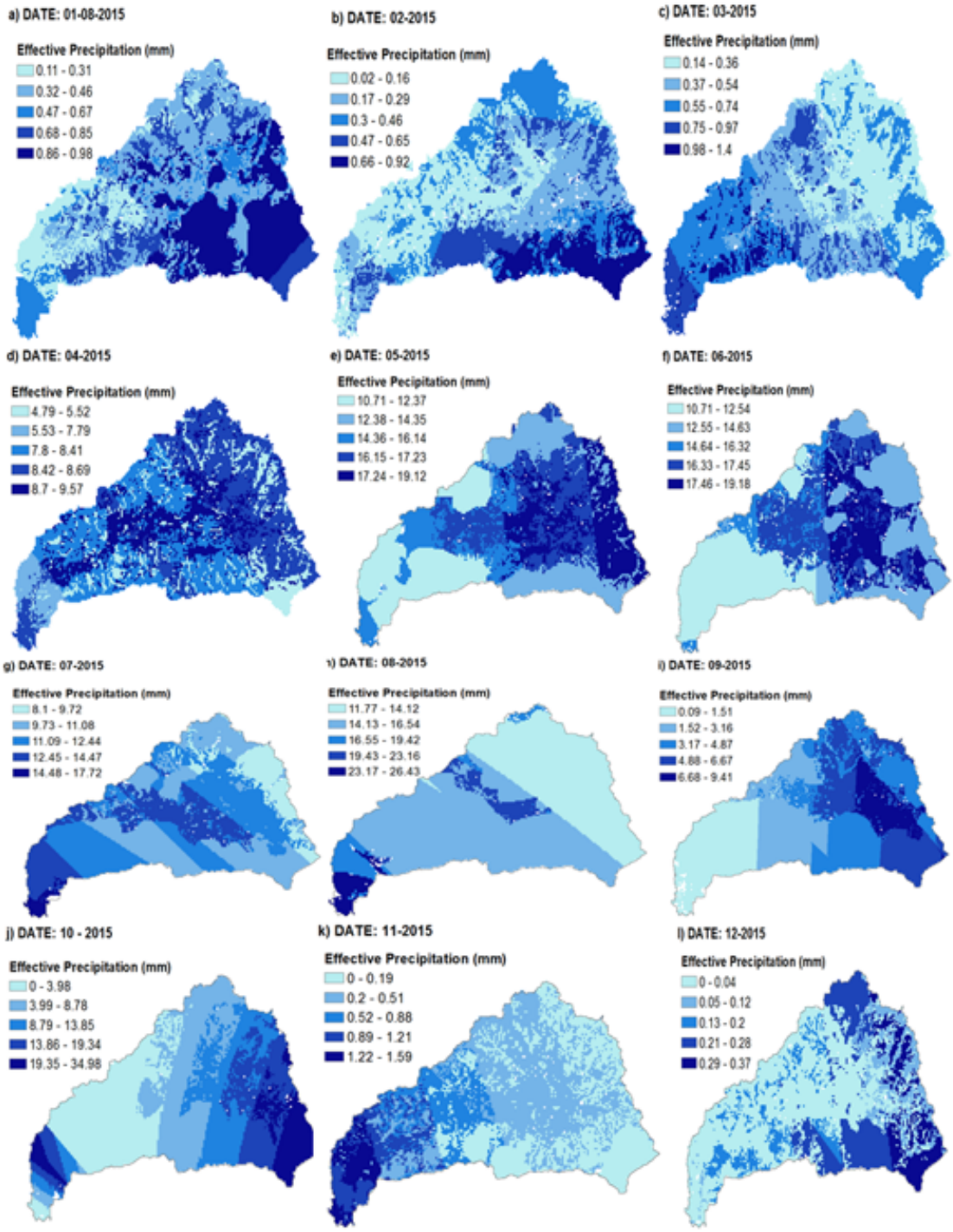

Figure 13: Effective precipitation (mm) in the Tucutunemo river basin, Aragua state, Venezuela, during 2015.

classified images are shown in Figure 8, where the land use an land cover (LULC) detected are five, the percent spatial distributions of LULC and C factor for April 2015 are the following (Figure 8d): 1) vegetation (18,92 km^2, 16%, 0,01), 2) agricultural (30,08 km^2 , 25%, 0,13), 3) degraded soil (69,95 km^2, 59%, 0,28), 4) clouds (0 km^2) and 5) shadows (0 km^2). The percent spatial distribution for August 2015 is the following (Figure 8h): 1) vegetation (106,93

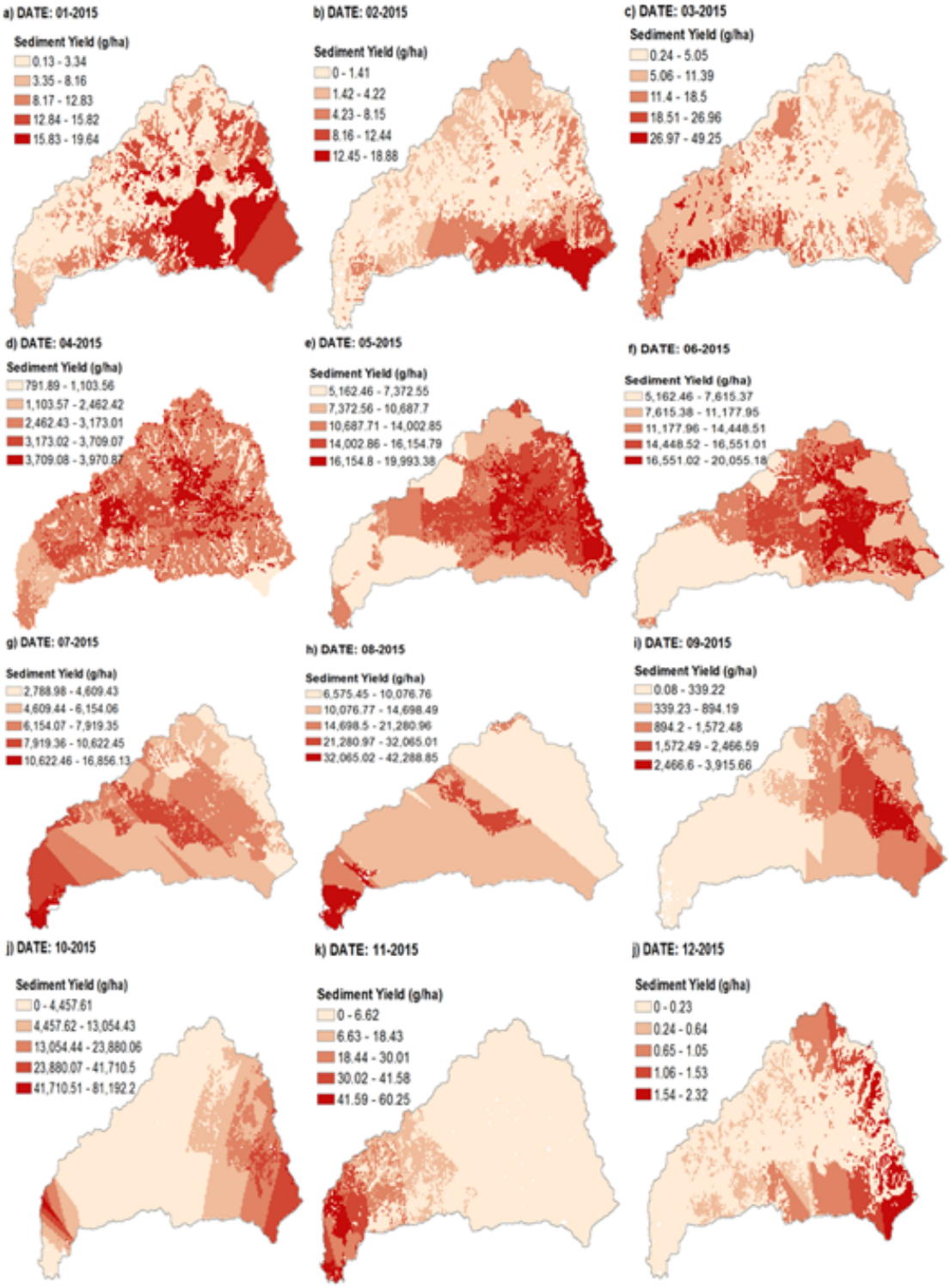

Figure 14: Sediment yield (g/ha) in the Tucutunemo river basin, Aragua state, Venezuela, during 2015.

km^2, 90,3%, 0,01), 2) agricultural (8,18 km^2, 6,9%. 0,13), 3) degraded soil (3,3 km^2, 2,78%, 0,28), 4) clouds (0 km^2) and 5) shadows (0 km^2).

e) Results of conservation practice factor (P) the results of P factor require los results obtained on the land cover and land use derived from Landsat 8 OLI satellite images (Figure 7). The classified images are shown in Figure 8, where

Table 5: Results of modeling of monthly precipitation statistical spatial prediction represented by the semivariances for the time series of images between 1986 and 1991 in the Tucutunemo river basin.

Date of Image	SSPM	Krigging Ordinario
2015-01-08	PC1 Semivariance SSPM	11,125·Nugget+28,328·J-Bessel(34977, 0,01)
	Predicted and Measured Regression function	0,389619308061585·x+4,12571115118064
	Standardized Error Regression Function	-0, 101338895899458 · x + 0, 700652314446477
	Samples	23
2015-02-09	PC1 Semivariance SSPM	3, 4597· Nugget+14,152·J-Bessel(31797, 0,70098)
	Predicted and Measured Regression function	0,421161923907274·x+3,1111196201193
	Standardized Error Regression Function	-0,132791502641185·x+0,816515041257734
	Samples	23
2015-03-13	PC1 Semivariance SSPM	10,456·Nugget+399,95·J-Bessel(499390, 10)
	Predicted and Measured Regression function	0,666064660774914·x+3,79913225011893
	Error Regression Function	-0,333935339225086·x+3,79913225011894
	Standardized Error Regression Function	-0,0533789679669054·x+0,680077588925542
	Samples	29
2015-04-30	PC1 Semivariance SSPM	124,86·Nugget+148,6·J-Bessel(93671, 0,01)
	Predicted and Measured Regression function	0,513132251301728·x+11,6236130675131
	Standardized Error Regression Function	-0,0363163911311564·x+0,710722861397881
	Samples	29
2015-05-16	PC1 Semivariance SSPM	97,385·Nugget+203,17·J-Bessel(558150, 1,0507)
	PMRF	0,526846690461996·x+9,823435814398
	SERF	-0,0433741481861566·x+0,890535529155565
	Samples	22
2015-06-17	PC1 Semivariance SSPM	119,36·Nugget+404,27·J-Bessel(220610, 1,4525)
	PMRF	0,549642947939819·x+15,5812696221036
	SERF	-0,0335424473779188·x+0,959696463418054
	Samples	26
2015-07-03	PC1 Semivariance SSPM	15,255·Nugget+492,47·J-Bessel(143030, 0,01)
	Predicted and Measured Regression function	0,751339936706698·x+12,8349520739822
	Error Regression Function	-0,248660063293302·x+12,8349520739822
	Standardized Error Regression Function	-0,03020683581146·x+1,48876217913642
	Samples	23
2015-08-04	PC1 Semivariance SSPM	104,77·Nugget+380,04·J-Bessel(153650, 0,01)
	Predicted and Measured Regression function	0,424297370730271·x+15,3072962029994
	Standardized Error Regression Function	-0,0311051114369269·x+0,741337510627896
	Samples	23
2015-09-05	PC1 Semivariance SSPM	89,603·Nugget+330·J-Bessel(69634, 0,01)
	Predicted and Measured Regression function	0,418660547119316·x+10,5186814140897
	Error Regression Function	-0,581339452880684·x+10,5186814140897
	Standardized Error Regression Function	-0,034164870671135·x+0,535457680012268
	Samples	21
2015-10-07	PC1 Semivariance SSPM	0·Nugget+472,76·J-Bessel(86277, 0,01)
	Predicted and Measured Regression function	0,427485456646955·x+10,5491971049236
	Standardized Error Regression Function	-0,109721002176278·x+2,02012098973276
	Samples	25
2015-11-24	PC1 Semivariance SSPM	131,07·Nugget+403,61·J-Bessel(275100, 0,79683)
	Predicted and Measured Regression function	0,432075908929093·x+10,6186075263914
	Error Regression Function	-0,567924091070908·x+10,6186075263914
	Standardized Error Regression Function	-0,0486290470209368·x+0,821683206330385
	Samples	28
2015-12-10	PC1 Semivariance SSPM	76,374·Nugget+254.73·J-Bessel(385490, 1,9944)
	Predicted and Measured Regression function	0,218247072662198·x+7,82057339541776
	Standardized Error Regression Function	-0,0492161823027591·x+0,58523883407058
	Samples	26

the land use an land cover (LULC) detected are five, the percent spatial distributions of LULC and P factor for April 2015 are the following (Figure 8d): 1) vegetation (18,92 km^2, 16%, 0,01), 2) agricultural (30,08 km^2 , 25%, 0,13), 3) degraded soil (69,95 km^2, 59%, 0,28), 4)

clouds (0 km^2) and 5) shadows (0 km^2). The percent spatial distribution for August 2015 is the following (Figure 8h): 1) vegetation (106,93 km^2, 90,3%, 0,8), 2) agricultural (8,18 km^2, 6,9%. 0,03), 3) degraded soil (3,3 km^2, 2,78%, 0,9), 4) clouds (0 km^2) and 5) shadows (0 km^2).

4.2 Results of estimation of the sediment yield (SY)

The results of monthly sediment yield maps during 2015 are obtained using equation (12). The results for the two factors involved in equation (12) are described for each one of these: a) Curve number (CN); and b) effective precipitation (Pe). The curve number used corresponds to the soil wet condition. The curve number varies between 85 and 89. This range of CN is small because the Tucutunemo river basin is of rural type. The curve number of 85 is associated to a good cover forest combined with a soil type with moderately high runoff potential. This curve number has the greatest occurrence because of the vegetation comprises the most part of terrain coverage in the Tucutunemo river basin, b) the effective precipitation (Pe) is influenced by the dry and rainy seasons occurred for 2015. The higher effective precipitation varies in the range between 19 y 34 mm for October 2015, which is located between the north and middle regions of the Tucutunemo river basin. During the dry season, the effective precipitation varies between 0 and 1,59 mm. During the rainy season, the effective precipitation varies between 9,57 and 34 mm. In whole year 2015, the effective precipitation is higher during the rainy season by comparing to the dry season, occurring in the agricultural plots and in the mountainous area, c) the sediment yield (SY) is influenced by the dry and rainy seasons occurred for 2015. The higher sediment yield varies in the range between 41710 and 81192 g/ha for October 2015, which is located between the north and middle regions of the Tucutunemo river basin. During the dry season, the sediment yield varies between 0 and 60,25 g/ha. During the rainy season, the sediment yield varies between 20055 and 81192 g/ha. In whole year 2015, the sediment yield is higher during the rainy season by comparing to the dry season, occurring in the agricultural plots and in the mountainous area.

4.3 Results of sediment delivery ratio (SDR)

The results of sediment delivery ratio (SDR) are shown in Figure 15. The sediment delivery ratio varies according to the dry or rainy season. In general, SDR varies between 0 and 1 in whole of year. However, SDR takes punctual values > 1 indicating accumulation areas of sediment. During the rainy season, it would be necessary to expand the number of classes to a number greater than ten to show the specific areas of sediment accumulation (Figures 15d-f).

5 Discussion

The soil erosion depends on six physical factors. The erosivity factor (R) is estimated from the kinetic energy for a precipitation intensity of 30 minutes. The precipitations of 30 minutes during the dry season are lower than 35 mm [10], corresponding to a type of precipitation that cause a dry condition of soil while the precipitation in the rainy season varies mainly between 35 and 50 mm, leaving a moderately high humidity in the soil. The precipitation events greater than 50 mm occur with lower frequency, three events were record in the months of July, August and October for 2015. These precipitation events transfer water to the matrix of the soil surface to reach a saturated condition in the porous spaces. In general, the precipitation of 30 minutes detaches the greatest soil amount in the rainy season. The erodibility factor (K) is greater in the inceptisols with respect to the mollisols. The structure of inceptisols having high sand and silt contents allows that the impact of the water drop detaches greater amount of soil particles by comparing with the mollisols in the middle and low part of Tucutunemo river basin. The slope length (L) factor is defined using a field slope length of 100 m, which is one dimension associated to the average length of the furrows in the agricultural plots [24]. The slope steepness (S) influences the negative or positive sign as an indicator of the direction of the water runoff on the terrain. The direction change direction is

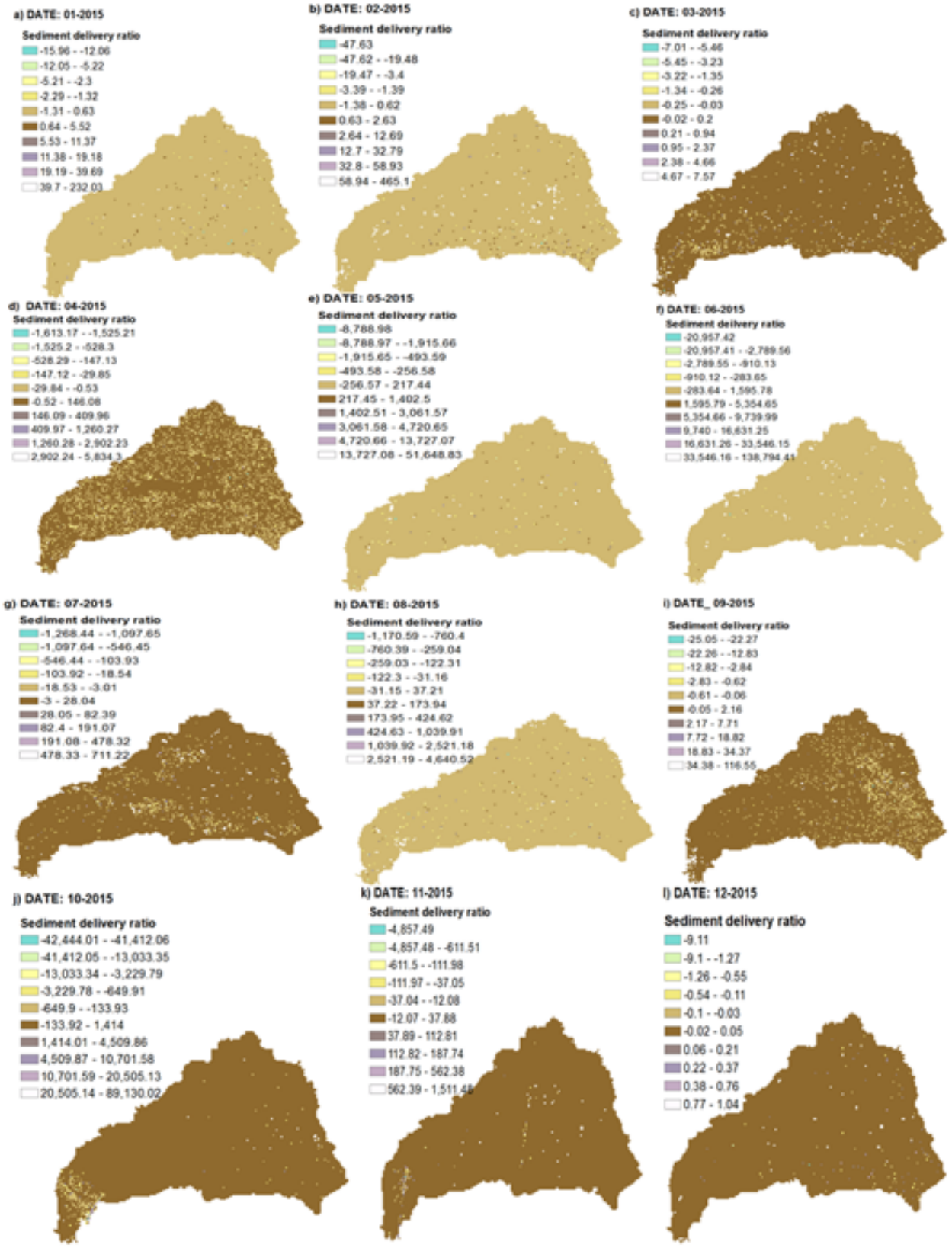

Figure 15: Monthly sediment delivery ratio (SDR) in the Tucutunemo river basin, Aragua state, Venezuela, during 2015.

significant in the mountains area of the Tucutunemo river basin. The crop management factor (C) and conservation practice (P) are dependent of the land use and land cover, the highest values are found where the agricultural plots are located in the Tucutunemo river basin, occurring to the middle and low part of basin. The soil erosion and sediment yield in the Tucutunemo river basin reach high values toward the high and middle part of the basin reducing the magnitude toward the low part. In addition, the magnitudes of the soil erosion and sediment yield are influenced by the dry and rainy seasons. The applied method for estimating the spatial distribution of soil erosion, sediment yield and SDR can detect the specific areas of sediment accumulation into the basin.

6 Conclusions

The Tucutunemo river basin is a rural area where the main land use and land cover are agricultural activities, vegetation and degraded soil. The agricultural activities are developed in the middle part of basin. By this study, it has been found that the soil erosion and yield sediment occur in the high and middle part of the basin. According the location, the precipitation of 30 minutes occurs in a magnitude from high moderately to high during the rainy season. The precipitation causes the greatest amount of soil erosion and sediment yield in the high and middle part of the basin where the soil is the inceptisols type, while these phenomenon are lower in the low part of basin where the mollisols is the soil type, which it is cohesive soil because of the clay contents. The spatial distribution of soil erosion and sediment yield leads to detect the localization of the specific areas of sediment accumulation into the basin.

7 Bibliography

[1] W.H. Wischmeier and D.D. Smith. Predicting Rainfall Erosion Losses. In *Agricultural Research Service Handbook 537*. US Department of Agriculture, 1978.

[2] K.G. Renard, G.R. Foster, G.A. Weesies, and J.P. Porter. RUSLE: revised universal soil loss equation. *Journal Soil and Water Conservation*, 46(1):30–33, 1991.

[3] J.R. Williams. The physical components of the EPIC model. In Sa. El-Swaify, WC. Moldenhauer, and A. Lo, editors, *Soil Erosion and Conservation*, pages 272–284. Ankeny, IA, 1985.

[4] D.B. Beasley, L.F. Huggins, and A. Monke. ANSWERS: A model for watershed planning. *Transactions of the ASAE*, 23(4):938–0944, 1980.

[5] D.C. Flanagan, J.C. Ascough, M.A. Nearing, and J.M. Laflen. The Water Erosion Prediction Project (WEPP) model. In RS. Harmon and WW. Doe, editors, *Landscape Erosion and Evolution Modelling*, pages 145–199. Kluwer Academic, New York, 2001.

[6] R.P.C. Morgan, J.N. Quinton, R.E. Smith, G. Govers, J.W.A. Poesen, K. Auerswald, G. Chisci, D. Torri, and M.E. Styczen. The European soil erosion model (EUROSEM): a process-based approach for predicting soil loss from fields and small catchments. *Earth Surface Processes and Landforms:The Journal of the British Geomorphological Research Group*, 23:527–544, 1998.

[7] N.S. Bulygina, M.A. Nearing, J.J. Stone, and M.H. Nichols. DWEPP: a dynamic soil erosion model based on WEPP source terms. *Earth Surface Processes and Landforms:The Journal of the British Geomorphological Research Group*, 32(7):998–1012, 2007.

[8] H.S. Gelagay and A.S. Minale. Soil loss estimation using GIS and Remote sensing techniques: A case of Koga watershed, Northwestern Ethiopia. *International Soil and Water Conservation Research*, 4(2):126–136, 2016.

[9] G. Singh and R.K. Panda. Grid-cell based assessment of soil erosion potential for identification of critical erosion prone areas using USLE, GIS and remote sensing: A case study in the Kapgari watershed, India. *International Soil and Water Conservation Research*, 5(3):202–211, 2017.

[10] E. Guevara and H. Cartaya. *Hidrología ambiental*. Consejo de Desarrollo Científico y Humanístico. Universidad de Carabobo, Valencia, Venezuela, 2004.

[11] D.G. Krige. A statistical approach to some basic mine valuation problems on the Witwatersrand. *Journal of the Southern African Institute of Mining and Metallurgy*, 52(6):119–139, 10520/AJA0038223X_4792, 1951.

[12] G. Metheron. Principles of geostatistics, economic geology. *Economic Geology*, 58(8):1246–1266, 1963.

[13] E.H. Isaaks and M.R. Srivastava. Applied geostatistics. Technical Report No. 551.72, ISA, 1989.

[14] G.R. Foster, D.K. McCool, K.G. Renard, and W.C. Moldenhauer. Conversion of the universal soil loss equation to SI metric units. *Journal of Soil and Water Conservation*, 36(6):355–359, 1981.

[15] R. Lal, J.M. Kimble, and T. Livari. *Soil degradation in the United States: extent, severity, and trends*. CRC Press, 2003.

[16] N. Parsamanesh, M. Zarrinkafsh, S.S. Shahoei, and W. Weisany. Evaluation of Distribution Functions

of Organic Carbon with Soil Depth in Vertisols and Inceptisols. *Bull. Env. Pharmacol. Life Sci*, 2(12):177–183, 2013.

[17] N. Voncir, Z.T. Kparmwang, A.A. Amba, and A.M. Hassan. Variation in Morphological Properties and Particle Size Distribution of Alfisols, Inceptisols and Entisols in the Gubi Soil Series, Bauchi, Nigeria. *Journal of Applied Sciences*, 6(13):2821–2824, 2006.

[18] J.M. Bremner and D.A. Genrich. Characterisation of the sand, silt, and clay fractions of some Mollisols. In *Soil Colloids and their Associations in Aggregates*, pages 423–438. Springer, Boston, MA, 1990.

[19] P.J. Ghiberto, S. Imhoff, P.L. Libardi, Ã.P.D. Silva, C.A. Tormena, and M.Ã. Pilatti. Soil physical quality of Mollisols quantified by a global index. *Scientia Agricola*, 72(2):167–174, 2015.

[20] T.W. Lambe and R.V. Whitman. *Soil mechanics SI version.* John Wiley & Sons, 2008.

[21] E.E. Sano, L.G. Ferreira, G.P. Asner, and E.T. Steinke. Spatial and temporal probabilities of obtaining cloud-free Landsat images over the Brazilian tropical savanna. *International Journal of Remote Sensing*, 28(12):2739–2752, 2007.

[22] L.E. Ramirez. Development of a Procedure for Determining Spacial and Time Variations of Precipitation in Venezuela. *Reports. Paper 145.*, 1971.

[23] D.E. Walling. The sediment delivery problem. *Journal of hydrology*, 65(1-3):209–237, 1983.

[24] S.K. Jain, S. Kumar, and J. Varghese. Estimation of soil erosion for a Himalayan watershed using GIS technique. *Water Resources Management*, 15(1):41–54, 2001.